7

Future of SiGe HBT Technology and Its Applications

M. Schröter[1,2], U. Pfeiffer[3] and R. Jain[3]

[1]Chair for Electron Devices and Integrated Circuits, Technische Universität Dresden, Germany
[2]Department of Electrical and Computer Engineering, University of California at San Diego, USA
[3]Institute for High-Frequency and Communication Technology (IHCT), University of Wuppertal, Germany

7.1 Introduction

The results of DOTSEVEN described in the previous chapters of this book mark a milestone in the development of SiGe HBT technology. This chapter reflects on how this milestone fits into the overall picture of semiconductor technologies with potential for high-speed/high-frequency applications. Furthermore, as any milestone is a temporary state, the possible future prospects of SiGe HBT device performance will be presented in terms of a roadmap. Finally, obstacles on the path toward the perceived performance limits of this technology are discussed.

7.2 Technology Comparison

Circuits operating at mm-wave frequencies have traditionally been implemented in III–V semiconductors due to the higher mobility in these materials. However, the high mobility occurs only at relatively low electric fields, which are easily exceeded under circuit-relevant bias conditions, especially when trying to generate high output power. Nevertheless, the fastest HBTs today have been fabricated in InP technology with the respective prototyping processes reaching (f_{T}, $f_{\max}$) values around (0.5, 1.1) THz for emitter widths of 130 nm [Urte11] and 200 nm [Bol16]. Compared to these

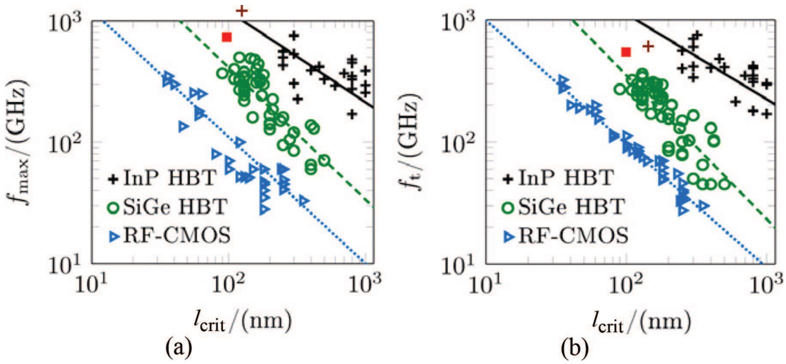

Figure 7.1 Operating speed comparison between SiGeC HBTs, InP HBTs, and MOSFETs vs. critical lithography dimensions (i.e., emitter width or channel length): (a) maximum oscillation frequency and (b) transit frequency. The lines represent LSQ fits of the data, the red filled squares DOTSEVEN results, and the larger crosses the best InP HBT data.

devices, DOTSEVEN SiGe HBTs with $(f_{\mathrm{T}}, f_{\max}) = (0.5, 0.72)$ THz are about one generation behind in terms of power gain cutoff frequency$_{\mathrm{x}}$. This performance difference is displayed in Figure 7.1, which includes f_{T} and $f_{\max}$ data of the three mainstream technology contenders gathered from many publications [Ros16]. The DOTSEVEN results have been marked by the red squares.

Although InP HBTs do have certain advantages over SiGeC HBTs such as higher breakdown voltage (at the same speed) and the potential of combined optical/electronic operation, it was shown in [Voi04] that "at comparable f_{T} and $f_{\max}$, there is very little difference in their performance in narrow-band mm-wave and in broadband and high-speed digital circuits"; i.e., for circuit applications, the advantage of the higher breakdown voltage in InP HBTs appears to be relatively small.

A main disadvantage of III–V technologies is their fairly low integration level and yield as well as the difficulty of structural downscaling due to strong surface recombination and the resulting low current gain. Hence, it will be difficult to leverage these technologies to their full extent to enable both more complex mm-wave systems and, in particular, mass-market wafer volume in the future. As a consequence, III–V material-based technologies do not achieve functionality and energy efficiency increases comparable to those of silicon technology, which in turn makes it difficult for them to compete also on cost. In addition, the relatively large process variations and the lack of accurate modeling tools have notoriously hampered (cost-) efficient III–V circuit design. Therefore, the III–V semiconductor industry and the related investment have been focused strongly on high-frequency/high-speed low-volume niche applications. The market success of more recent approaches toward a heterogeneous integration with completed CMOS wafers (e.g., [Ram12]) remains unclear yet. Among the issues are certainly the very different process qualification criteria in the silicon (especially the digital CMOS) world and in the III–V world.

According to Figure 7.1 the cutoff frequencies of the best RF-CMOS processes come close to those of SiGe HBTs, but at the expense of a significantly more advanced lithography, typically at least three lithography nodes. Achieving the DOTSEVEN results though would require a CMOS process with about a 14 nm channel length (which does not correspond to the 14 nm node!), assuming that progress in device speed continues for CMOS as sketched by the corresponding dashed line in Figure 7.1. As will be discussed later below, this assumption is unlikely to be the case.

The considerations so far have centered around *device*-related operating frequencies. However, in a circuit the transistors are connected to other devices, which along with the connection represent more or less large capacitive, inductive, and resistive loads. For instance, high-quality passive devices for RF applications have to be placed in the uppermost metalization levels. Figure 7.2(a) displays a 3D view of a typical connection between a transistor and the upper metal layer. The impact of this connection on transistors having the same speed after deembedding (about 300 GHz) is shown in Figure 7.2(b): the MOSFET's f_T decreases by about a factor of two, while the HBT looses

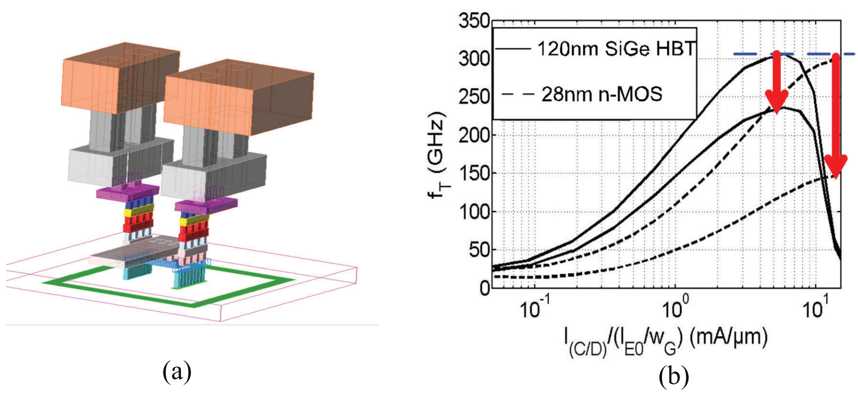

Figure 7.2 Impact of device connections to other circuit elements (a) on the transit frequency of a SiGeC HBT with 120 nm emitter window width and a MOSFET of the 28 nm node (b). The upper lines in (b) represent the pad and pad-device connection line deembedded data, while the lower lines represent the un-deembedded data.

about 20% of its speed. Similar observations have been noted in [Ina11], where the peak operating frequencies ($f_\mathrm{T}, f_\mathrm{max}$) of 45 nm MOSFETs drop by a factor of two, once the metallization necessary for building circuits is included. The reason why HBTs do not show this severe deterioration is their much higher transconductance g_m and corresponding drive capability. In other words, devices with the same ratio of g_m and input capacitance have the same f_T, but devices with a higher g_m will fundamentally fare better in circuits since the device capacitance there will only be a more or less small fraction of the total capacitance.

Based on the observations described above, it is therefore instructive to look at the values of g_m when comparing process technology performance, since g_m represents a better indication of achievable circuit speed. Figure 7.3 shows the measured and predicted values of g_m for a variety of incumbent and emerging process technologies. For comparison, g_m has been normalized to emitter length (for HBTs), gate width (for planar MOSFETs), or channel perimeter length (for nano-wire and -tube FETs[1]). It is clearly visible that HBTs have a much higher transconductance per finger length than FETs. Furthermore, FETs appear to be unable to ever catch up to HBTs in terms of transconductance, even when assuming ideal performance scaling according to the approximation of existing data (dashed lines).

Figure 7.3 also includes the transconductance values for future technology nodes, which have been predicted based on detailed TCAD simulations and compact models for complete 3D transistors with all relevant parasitics included [Sch17, Voi17] and have become the basis for the 2014 and 2015 ITRS tables. For MOSFETs, the peaks of g_m (around 4 mS/μm) and f_T (around 600 GHz) are predicted for a channel length of 10 nm, while beyond that length the strong impact of surface scattering in the extremely thin channel layer will lead to a drastic decrease (to, e.g., $g_\mathrm{m} \approx 1.5$ mS/μm, $f_\mathrm{T} \approx 200$ GHz). This is in stark contrast to HBT scaling, which significantly benefits from smaller dimensions in all aspects of electrical performance until a critical base width is reached and the small emitter area leads to a high emitter contact resistance.[2] The ultimate performance of SiGe HBTs was investigated in [Sch11a, Sch11b] using detailed TCAD simulation and

[1]Normalizing to the perimeter takes into account (roughly) that screening effects would lead to a lower g_m value if the wires or tubes were placed next to each other, which would correspond to a normalization to the diameter (or minimum footprint for a gate-all-around channel).

[2]Note though that the impact of contact resistances increases with smaller device dimensions in all technologies and becomes visible first in highly scaled FETs.

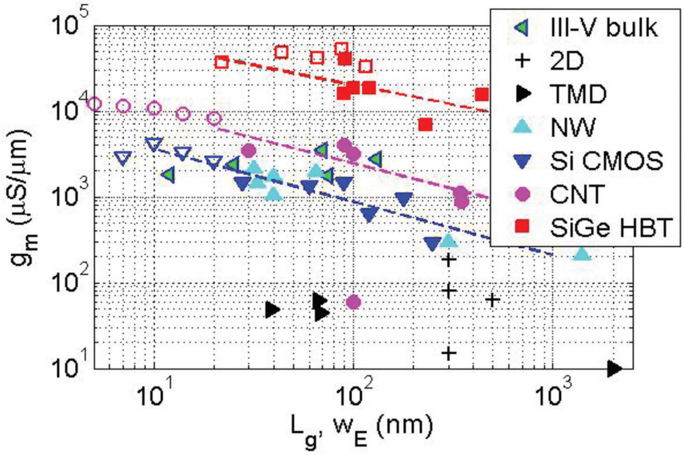

Figure 7.3 Comparison of the terminal (or extrinsic) transconductance of transistors from a large variety of process technologies. Filled symbols represent measured data and open symbols represent predicted (roadmap) data. For FETs, the legend designations correspond to the channel material and structure: planar III–V such as InGaAs (III–V bulk); planar single- or few atomic layers such as black phosphorus or germanane (2D); planar transition metal dichalcogenide such as MoS_2 (TMD); planar or FinFET silicon (Si-CMOS); nano-wire silicon or III–V (NW); carbon nano-tube (CNT).

accurate compact models with all known physical effects and device-related parasitics included. The predictions resulted in a transit frequency between 0.8 and 1 THz and maximum oscillation frequency around 2 THz, depending on the assumed contact resistivities especially for the emitter. For the ITRS tables (see also [Sch17] for more details), quite conservative values have been assumed, which lead to somewhat reduced device operating frequencies and transconductances compared to [Sch11b].

The doping profile of the technology node N3, the performance of which was predicted in 2013, served as the guideline for the DOTSEVEN process development. During process development, accurate physics-based model parameters were determined based on which the evaluation of the impact of the various physical and parasitic effects on device performance [Kor15, Paw17] is possible. This strategy provided valuable insight for prioritizing the process development tasks. It is interesting to note that the electrical parameters, such as base sheet resistance and capacitance per area, of the final process version of DOTSEVEN meet those of the roadmap node N3 predicted earlier quite well. This validates the accuracy of the predictions and the employed approach.

The predicted progress in device speed is closely linked to the increase in current densities required for achieving peak operating frequencies. The corresponding transconductance at the device terminals is more or less strongly reduced by the emitter series (contact) resistance. With conservative assumptions about contact resistivities, transconductance values of at least 40 mS/μm can be expected according to Figure 7.3 at the present end of the roadmap. This value remains an order of magnitude higher than that predicted for the best MOSFETs and also still higher than that predicted for the best CNTFETs by a factor of four. Notice that due to the lack of sufficient hardware, the predictions of the latter are associated with much higher uncertainty than those for MOSFETs.

An important aspect for mm-wave and THz applications is the achievable output power at a given frequency. For advanced MOSFET technologies, the latter is impacted significantly by the decrease of the voltage gain, which is caused by the increased output leakage and associated output conductance. HBTs do not show this decrease unless they are scaled (vertically) beyond the last node presently shown in the ITRS tables. Output power can also be increased with device size. While this increases the device-related capacitances in both HBTs and MOSFETs, an increase in emitter length alone reduces all series resistances in HBTs but a corresponding gate width increase in FETs leads to a larger gate resistance. Moreover, the maximum allowed drain–source voltage in advanced RF-MOSFETs is lower than the maximum collector–emitter voltage in advanced high-speed HBTs. Increasing the number of parallel devices in MOSFET-based power amplifiers leads to larger interconnect parasitics per unit drain width, while stacked power amplifier architectures require a larger number of devices and thus again more passives and parasitics per unit drain width. Another important building block in (sub-)mm-wave systems is the VCO. Its phase noise strongly depends on the flicker ($1/f$) noise of the transistors. Here, HBTs have much lower corner frequencies than MOSFETs, in which $1/f$ noise keeps increasing for more advanced nodes. Overall, HBTs appear to have a distinctive advantage in the area of mm-wave and THz amplifiers from a technical circuit design perspective.

Finally, a few words on cost. With the development and added masks for the required RF-passives, an RF-CMOS process becomes significantly more costly than the corresponding digital process. Thus, a depreciated CMOS process with high-speed SiGe HBTs integrated (i.e., a BiCMOS process) can often be cheaper and thus very cost competitive to advanced RF-CMOS. Such a BiCMOS process not only provides better RF front-end performance (in terms of analog HF features and energy efficiency) but is also earlier available on the market. In view of these aspects, RF-CMOS based on an advanced node makes sense only for applications that require (i) higher digital functionality and density than an already available BiCMOS process with comparable front-end (i.e., HBT) performance and (ii) very high product volume.

Due to the already existing large investment and associated infrastructure in 200 and 300 mm silicon wafer fabs around the world, SiGe:C HBTs with operating speed in the THz range are desirable. Implemented into depreciated (and hence low-cost) digital CMOS platforms, the associated SiGe:C BiCMOS single-chip technologies are capable of covering (at reasonable wafer cost) medium- and large-volume applications with mm-wave and THz analog front-ends, which would be either far too expensive when implemented in most advanced CMOS technology or would not even be possible to realize there due to the inferior analog characteristics of future advanced MOSFETs as discussed above. Therefore, a relatively small investment in SiGe:C HBT process development will yield large gains in terms of (ultimately commodity) market coverage.

7.3 Future Millimeter-wave and THz Applications

The terahertz or sub-millimeter frequency range, roughly defined as extending from 300 GHz to 3 THz, has so far resisted attempts to broadly harness its potential for everyday applications. This led to the expression THz gap, loosely describing the lack of adequate technologies to effectively bridge this transition region between microwaves and optics – both readily accessible via well-developed electronic and laser-based approaches – by, e.g., integrated and cost-efficient electronics. THz technology is an emerging field which has demonstrated a wide-ranging potential. Extensive research in the last years has identified many attractive application areas and paved the technological path toward broadly usable THz systems. THz technology is currently in a pivotal phase and will soon be able to radically expand our analytic capabilities via its intrinsic benefits.

Applications of mm-wave and THz frequencies led by the silicon integrated technologies can be subdivided into communication, radar, imaging, and sensing areas, as illustrated in Figure 7.4. In the following sections, we describe some of these applications and the recent, state-of-the-art hardware developments in the corresponding areas as it relates to DOTSEVEN.

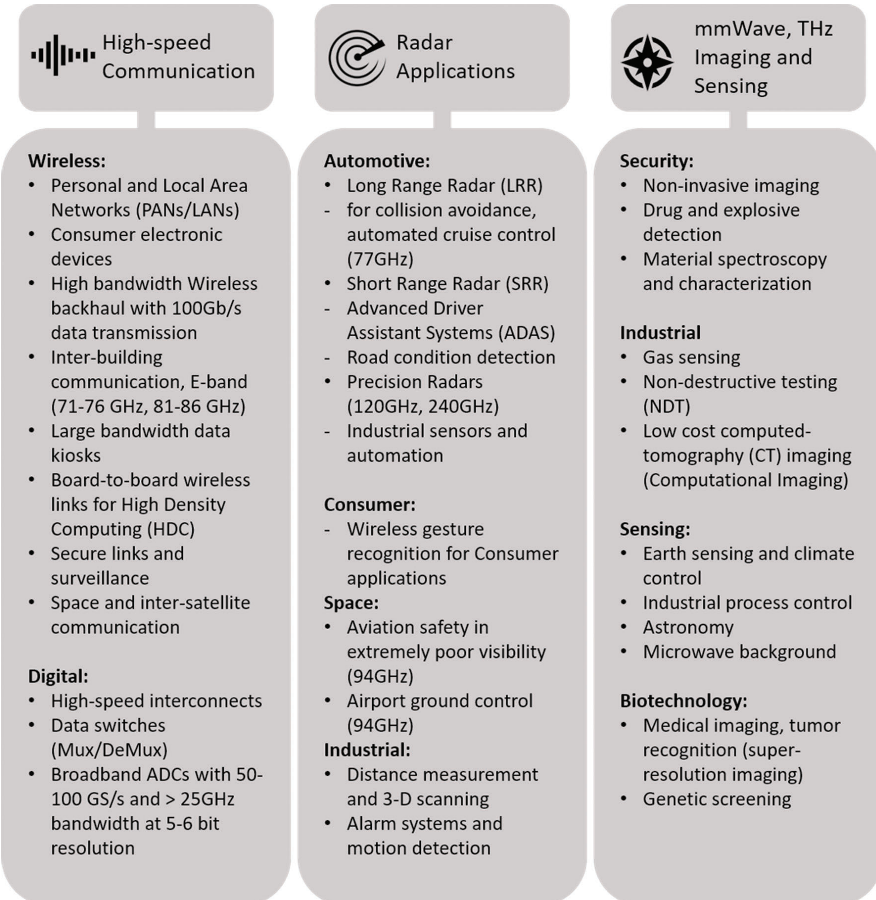

Figure 7.4 Potential applications for silicon integrated mm-wave and THz circuits.

7.3.1 Communication

To improve the data capacity beyond 10 Gbps for wireless transmission, improving the spectral efficiency with advanced modulation schemes is no longer sufficient and higher bandwidth becomes an absolutely necessity. The mm-wave and THz bands, due to their large relative bandwidth, show great potential for future wireless communication [Son11]. Such large frequencies, however, suffer from greater atmospheric attenuation as compared to the traditional radio waves. Still, the atmospheric windows near 90 GHz, 140 GHz, and 240 GHz are being considered for future communication and radar applications [Fed10].

Due to a larger atmospheric attenuation, the THz waves are expected to be first used for indoor wireless personal-area (WPAN) and local-area (WLAN) networks, where the range is limited to a few tens of meters at the most. Along with the high-capacity, the high directivity of THz waves is also considered as an advantage to ensure secure (requiring line-of-sight) or high-density, non-interfering data networks. Some of the possible applications of THz communication are:

1. Wireless distribution of HDTV content in an in-home network. While the current 60 fps, progressive full HD (1080p60) content requires data transmission rates near 3 Gbps, future ultra HD 8K content would require wireless data transmission rates in the ballpark of 24 Gbps [Son11].
2. High-bandwidth wireless backhauls in high-density mesh multipoint to point/multipoint (first-mile and last-mile) networks may require data rates reaching 100 Gbps.
3. Rapid uploading and downloading of large files from a server which can serve as a public data kiosk.
4. Inter- and intra-building communication networks for manufacturing floor automation, etc.

Silicon–germanium HBT technology is driving the front-end development for mm-wave and THz bands, and several key components as well as fully integrated transceiver systems have been demonstrated. Figure 7.5 shows the output power versus frequency for some recently published SiGe mm-wave/THz sources. A 0.53 THz, 0 dBm free-space radiating source composed of 16 on-chip, non-locked radiating pixels, each with a differential triple-push oscillator (TPO) and on-chip ring antenna, was demonstrated in [Pfe14]. A similar, single-ended TPO design for a single 0.49 THz radiator was also shown in [Hil15]. [Hil17] demonstrated another approach of using a fundamental differential Colpitts oscillator with second harmonic extraction at 215 GHz and feeding it to a frequency doubler for 430 GHz signal radiation with –6.3 dBm of output power.

Cascaded multiplier chains with larger multiplication factors have also been demonstrated. In this approach, an external, phase-stable signal is fed to the multiplier chain to generate the THz signal. In [Eri11], the $\times 18$ multiplier chain consists of two cascaded tripler stages followed by a balanced doubler and shows a peak output power of –3 dBm at 325 GHz.

Further signal amplification is done by on-chip integrated power amplifiers (PAs). In [Nee13], a 160 GHz PA with 20 dB gain and 10 dBm

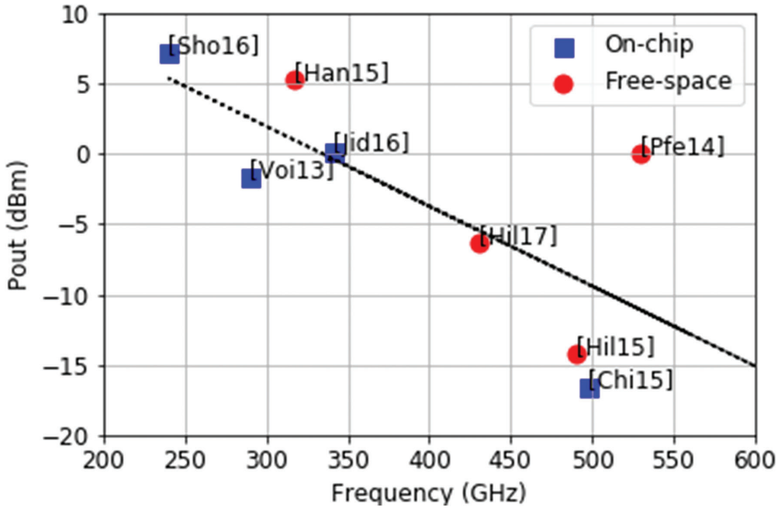

Figure 7.5 Frequency versus output power of some recently published SiGe integrated mm-wave/THz sources.

saturated output power (P_{sat}) was demonstrated. A parallel power-combination approach with four PA cores was used in [Nee16] to show 25 dB gain and 9 dBm P_{sat} for 200–225 GHz.

In the recent years, fully integrated silicon RF front-ends operating above 200 GHz have become feasible due to the continuous technology improvement. Both CMOS [Kan15, Thy15, Par12, Tak17] and SiGe [Fri17, Rod17, Rod18] front-ends have been reported in the literature. Circuits using sub-harmonic techniques with doubler or tripler as last stage before the antenna like a 240 GHz transceiver chipset utilizing QPSK in 65 nm CMOS can be found in the combination of [Kan15] and [Thy15]. A 260 GHz OOK transceiver in 65 nm bulk CMOS was reported in [Par12]. [Tak17] presents a CMOS transmitter working at 300 GHz capable of communicating over 5 cm at 56 Gbps. A complete SiGe chipset for 50 Gbps at mm distance is presented by [Fri17]. In [Rod17], a SiGe integrated 240 GHz transceiver chipset in the DOTSEVEN technology (as detailed in Chapter 6) is reported with a data-rate of 50 Gbps communicating over 100 cm distance. The data rate was further improved to 65 Gbps by post-process IF filtering at the receiver-end in [Rod18]. A comparison of these front-ends is presented in Table 7.1. Extensive research in device technology and circuits continues to improve the performance further, indicating that SiGe HBTs are becoming a formidable

Table 7.1 Si-integrated wireless communication links above 200 GHz

Reference	Frequency [GHz]	Tx/Rx	Data [Gbps]	Error (Modulation)	Distance
[Kan15]	240	Tx	16	–	–
[Thy15]	240	Rx	10/16	BER $< 10^{-6}$ $/10^{-4}$ (QPSK)	–
[Par12]	260	Tx, Rx	14	– (OOK)	4 cm
[Fri17]	190	Tx, Rx	50	BER $< 10^{-3}$ (BPSK)	0.6 cm
[Rod17]	240	Tx, Rx	50	EVM 29% (QPSK)	100 cm
[Tak17]	300	Tx	56	EVM 13.4% (16 QAM)	5 cm
[Rod18]	240	Tx, Rx	65	BER $<10^{-4}$ (QPSK)	100 cm

alternative to III–V technologies for mm-wave and THz communication, and SiGe HBT technology is quickly extending toward 100 Gbps data-rates.

7.3.2 Radar

Radar systems are used for distance and velocity sensing, and they also benefit by moving to higher frequencies. A larger available absolute bandwidth at higher frequencies improves the overall range resolution. Also, higher frequencies allow for compact radar apertures.

One extremely popular commercial usage for high-frequency radars is for automotive applications with 76–77 GHz and 79–81 GHz allocated frequency bands. These automotive radars are being considered for a wide range of Advance Driver Assist Systems (ADAS), including (i) long-range (high-directivity, narrow forward looking beam) systems for applications such as adaptive cruise control, (ii) medium-range (medium directivity, beam-width) systems for applications such as cross-traffic alert, and (iii) short-range (direct proximity) systems for applications such as obstacle avoidance and parking assist. While such systems are already deployed at present [Has12], continuous improvement in technology would allow for a better performance (power consumption/noise figure), ultimately leading to a cost reduction and improved reliability. Similarly, 94 GHz constitutes another frequency band which is popular for aerospace and aviation radars, for application such as for displaying runway image in poor weather conditions [Gos09], for airport ground control systems [Mar16], and weather-cloud investigations [Mar08].

Even higher frequencies allow for millimeter-range resolution. Such precision radars can be used for industrial imaging, inspection, and automation. In addition, novel consumer applications such as gesture recognition [Arb13], [GSoli] have also started to emerge.

Due to a similar coherent nature, the hardware advancements discussed for the communication chipsets also benefit the radar systems similarly. Within the frame of the DOTSEVEN project, a complete highly integrated FMCW homodyne monostatic radar system operating around 240 GHz with a 60 GHz bandwidth and a state-of-the-art 2.57 mm range resolution was developed [Statn15]. The radar module was used for 3-D imaging of cardboard boxes with a dynamic range of around 50 dB in the acquired range profiles. Key to the success of silicon technologies is a low-cost packaging scheme which needs to be developed to support low cost on the sub-component level. Hence, the DOTSEVEN radar chips were further packaged together with wideband lens-integrated on-chip annular-slot antenna [Grzyb15] and wire bonded onto a low-cost FR4 printed-circuit board.

7.3.3 Imaging and Sensing

Three-dimensional THz imaging based on the principle of computed tomography (THz-CT) is one of the emerging applications that may be explored in commercial imaging and sensing applications. THz-CT offers volumetric object reconstruction with an image contrast based on the characteristic THz absorption of the illuminated material. Since THz radiation is non-ionizing and thus requires no dedicated safety measures, THz-CT represents an interesting alternative to X-ray technology for low-cost industrial quality control. A THz-CT system solely based on components built in DOTSEVEN technology was built and evaluated. A SiGe-HBT source [Hill15] was focused in the object plane and refocused to an NMOS [Jain16] detector with low-cost PTFE lenses. The 3D image was reconstructed from measurements at multiple projection angles and positions based on a filtered back-projection algorithm. The system offers a dynamic range of up to 60 dB at 490 GHz. The Gaussian beam waist sizes are 2.54 mm in the y-direction and 2.40 mm in the z-direction. These results show that Terahertz 3D CT imagers can be entirely implemented in a silicon process technology.

References

[Arb13] Arbabian, A., Callender, S., Kang, S., Rangwala, M., and Niknejad, A. M. (2013). A 94 GHz mm-wave-to-baseband pulsed-radar transceiver with applications in imaging and gesture recognition. *IEEE J. Solid State Circ.* 48, 1055–1071.

[Bol16] Bolognesi, C. R., Flückinger, R., Alexandrova, M., Quan, W., Lövblom, R., and Ostinelli, O. (2016). InP/GaAsSb DHBTs for THz applications and improved extraction of their cutoff frequencies. *IEDM Tech. Digest* 6, 723–726.

[Eri11] Ojefors, E., Heinemann, B., and Pfeiffer, U. R. (2011). Active 220- and 325 GHz frequency multiplier chains in an SiGe HBT technology. *IEEE Trans. Microw. Theory Tech.* 59, 1311–1318.

[Fed10] Federici, J., Moeller, L. (2010). Review of terahertz and subterahertz wireless communications. *J. Appl. Phys.* 107, 111101.

[Fri17] Fritsche, D., Stärke, P., Carta, C., and Ellinger, F. (2017). A low-power SiGe BiCMOS 190 GHz transceiver chipset with demonstrated data rates up to 50 Gbit/s using on-chip antennas. *IEEE Trans. Microw. Theory Tech.* 65, 3312–3323.

[Gos09] Goshi, D. S., Liu, Y., Mai, K., Bui, L., and Shih, Y. (2009). "Recent advances in 94 GHz FMCW imaging radar development," in *Proceedings of the 2009 IEEE MTT-S International Microwave Symposium Digest*, Boston, MA, 77–80.

[Grzyb15] Grzyb, J., Statnikov, K., Sarmah, N., and Pfeiffer, U. R. (2015). "A broadband 240 GHz lens-integrated polarization-diversity on-chip circular slot antenna for a power source module in SiGe technology," in *Proceedings of the 45th European Microwave Conference (EuMC)*, Paris, 570–573.

[GSoli] Project Soli (2017). Available at: https://atap.google.com/soli/ accessed November 1, 2017.

[Has12] Hasch, J., Topak, E., Schnabel, R., Zwick, T., Weigel, R., and Waldschmidt, C. (2012). Millimeter-wave technology for automotive radar sensors in the 77 GHz frequency band. *IEEE Trans. Microw. Theory Tech.* 60, 845–860.

[Hil15] Hillger, P., Grzyb, J., Lachner, R., and Pfeiffer, U. (2015). "An antenna-coupled 0.49 THz SiGe HBT source for active illumination in terahertz imaging applications," in *Proceedings of the 2015 10th European Microwave Integrated Circuits Conference (EuMIC)*, Paris, 180–183.

[Hill15] Hillger, P., Grzyb, J., Lachner, R., and Pfeiffer, U. (2015). "An antenna-coupled 0.49 THz SiGe HBT source for active illumination in terahertz imaging applications," in *Proceedings of the 2015 10th European Microwave Integrated Circuits Conference (EuMIC)*, Paris, 180–183.

[Ina11] Inac, O., Cetinoneri, B., Uzunkol, M., Atesal, Y., and Rebeiz, G. M. (2011). "Millimeter-wave and THz circuits in 45 nm SOI CMOS," in *Proceedings of the Compound Semiconductor Integrated Circuit Symposium [CSICS]* (Rome: IEEE), 1–4.

[Jain16] Jain, R., Rücker, H., and Pfeiffer, R. (2016). "Zero gate-bias terahertz detection with an asymmetric NMOS transistor," in *Proceedings of the 2016 41st International Conference on Infrared, Millimeter, and Terahertz Waves (IRMMW-THz)*, Copenhagen, 1–2.

[Kan15] Kang, S., Thyagarajan, S. V., and Niknejad, A. M. (2015). A 240 GHz fully integrated wideband QPSK transmitter in 65 nm CMOS. *IEEE J. Solid State Circ*. 50, 2256–2267.

[Kor15] Korn, J., Ruecker, H., Heinemann, B., Pawlak, A., Wedel, G., and Schroter, M. (2015). "Experimental and theoretical study of fT for SiGe HBTs with a scaled vertical doping profile," in *Proceedings of the IEEE BCTM*, Boston, 117–120.

[Mar08] Marchand, R., Mace, G. G., Ackerman, T., and Stephens, G. (2008) "Hydrometeor detection using cloudsat—an earth-orbiting 94 GHz cloud radar. *J. Atmos. Oceanic Technol.* 25, 519–533.

[Mar16] Martinez, A., Lort, M., Aguasca, A., and Broquetas, A. (2015). "Submillimetric motion detection with a 94 GHZ ground based synthetic aperture radar," in *Proceedings of the IET International Radar Conference 2015*, Hangzhou, 1–5.

[Nee13] Sarmah, N., Chevalier, P., and Pfeiffer, U. R. (2013). 160 GHz power amplifier design in advanced SiGe HBT technologies with Psat in excess of 10 dBm. *IEEE Trans. Microw. Theory Tech*. 61, 939–947.

[Nee16] Sarmah, N., Aufinger, K., Lachner, R., and Pfeiffer, U. R. (2016). "A 200–225 GHz SiGe power amplifier with peak Psat of 9.6 dBm using wideband power combination," in *Proceedings of the ESSCIRC Conference 2016: 42nd European Solid-State Circuits Conference*, Lausanne, 193–196.

[Par12] Park, J. D., Kang, S., Thyagarajan, S. V., Alon, E., and Niknejad, A. M. (2012). "A 260 GHz fully integrated CMOS transceiver for wireless chip-to-chip communication," in *Proceedings of the 2012 Symposium on VLSI Circuits (VLSIC)*, Honolulu, HI, 48–49.

[Paw17] Pawlak, A., Heinemann, B., Schröter, M. (2017). "Physics-based modeling of SiGe HBTs with fT of 450 GHz with HICUM Level 2," in *Proceedings of the IEEE BCTM*, Miami, FL, 134–137.

[Pfe14] Pfeiffer, U. R. et al. (2014). A 0.53 THz reconfigurable source module with up to 1 mW radiated power for diffuse illumination in terahertz imaging applications. *IEEE J. Solid State Circ.* 49, 2938–2950.

[Ram12] Raman, S., Dohrmann, C., and Chang, T.-H. (2012). "Heterogeneous BiCMOS technologies and circuits and the DARPA DAHI program," in *Proceedings of the IEEE BCTM*, Portland, OR, 127–132.

[Rod17] Vazquez, P. R., Grzyb, J., Sarmah, N., Pfeiffer, U. R., and Heinemann, B. (2017). "Towards THz high data-rate communication: a 50 Gbps all-electronic wireless link at 240 GHz," in *Proceedings of the 4th ACM International Conference on Nanoscale Computing and Communication*, Washington DC.

[Rod18] Rodriguez Vazquez, P., Grzyb, J., Sarmah, N., Heinemann, B., and Pfeiffer, U. R. (2018). *A 65 Gbps QPSK One Meter Wireless Link Operating at a 225–255 GHz Tunable Carrier in a SiGe HBT Technology*. Anaheim, CA: RWW.

[Ros16] Rosenbaum, T. (2017). *Performance Prediction of a Future SiGe HBT Technology using a Heterogeneous Set of Simulation Tools and Approaches*. Ph.D. dissertation, TU Dresden, Dresden.

[Sch11a] Schroter, M., Wedel, G., Heinemann, B., Jungemann, C., Krause, J., Chevalier, P., and Chantre, A. (2011). Physical and electrical performance limits of high-speed SiGeC HBTs – Part I: vertical scaling. *IEEE Trans. Electron Dev*. 58, 3687–3696.

[Sch11b] Schroter, M., Krause, J., Rinaldi, N., Wedel, G., Heinemann, B., Chevalier, P., et al. (2011). Physical and electrical performance limits of high-speed SiGeC HBTs – Part II: lateral scaling. *IEEE Trans. Electron Dev*. 58, 3696–3706.

[Sch17] Schröter, M., Rosenbaum, T., Chevalier, P., Heinemann, B., Voinigescu, S., Preisler, E., et al. (2017). SiGe HBT technology: future trends and TCAD based roadmap. *Proc. IEEE* 105, 1068–1086.

[Son11] Song, H. J., and Nagatsuma, T. (2011). Present and future of terahertz communications. *IEEE Trans. Terahertz Sci. Technol.* 1, 256–263.

[Statn15] Statnikov, K., Grzyb, J., Sarmah, N., Malz, S., Heinemann, B., and Pfeiffer, U. R. (2015). A 240 GHz circularly polarized FMCW radar based on a SiGe transceiver with a lens-coupled on-chip antenna. *Int. J. Microw. Wireless Technol.* 8, 1–9.

[Tak17] Takano, K., Katayama, K., Amakawa, S., Yoshida, T., and Fujishima, M. (2017). "56 Gbit/s 16 QAM wireless link with 300 GHz-band CMOS transmitter," in *Proceedings of the 2017 IEEE MTT-S International Microwave Symposium (IMS)*, Honolulu, HI, 793–796.

[Thy15] Thyagarajan, S. V., Kang, S., and Niknejad, A. M. (2015). A 240 GHz fully integrated wideband QPSK receiver in 65 nm CMOS. *IEEE J. Solid State Circ*. 50, 2268–2280.

[Urt11] Urteaga, M., Pierson, R., Rowell, P., Jain, V., Lobisser, E., and Rodwell, M. J. W. (2011). "130nm InP DHBTs with *ft* >0.52THz and *fmax* >1.1THz," in *Proceedings of the 69th Development Research Conference*, Washington, DC, 281–282.

[Voi04] Voinigescu, S. P., Dickson, T. O., Beerkens, R., Khalid, I., and Westergaard, P. (2004). "A comparison of si CMOS, SiGe BiCMOS, and In P HBT technologies for high-speed and millimeter-wave ICs," in *Proceedings of the Topical Meeting Silicon Monolithic Integrate Circuits in RF Systems*, Austin, TX, 111–114.

[Voi17] Voinigescu, S. P., Shopov, S., Bateman, J., Farooq, H., Hoffman, J., Vasilakopoulos, K. (2017). Silicon millimeter-wave, terahertz, and high-speed fiber-optic device and benchmark circuit scaling through the 2030 ITRS horizon. *Proc. IEEE* 105, 1087–1104.